The Astrophysical Journal, 686:1292–1301, 2008 October 20

ACCRETION AND DESTRUCTION OF PLANETESIMALS IN TURBULENT DISKS

Shigeru Ida
Tokyo Institute of Technology, Ookayama, Meguro-ku, Tokyo 152-8551, Japan; ida@geo.titech.ac.jp

and

Tristan Guillot and Alessandro Morbidelli
Observatoire de la Côte d'Azur, CNRS UMR 6202, BP 4229, 06304 Nice Cedex 4, France; guillot@oca.eu, morby@oca.eu
Received 2008 May 25; accepted 2008 July 10

ABSTRACT

We study the conditions for collisions between planetesimals to be accretional or disruptive in turbulent disks, through analytical arguments based on fluid dynamical simulations and orbital integrations. In turbulent disks, the velocity dispersion of planetesimals is pumped up by random gravitational perturbations from density fluctuations of the disk gas. When the velocity dispersion is larger than the planetesimals' surface escape velocity, collisions between planetesimals do not result in accretion and may even lead to their destruction. In disks with a surface density equal to that of the "minimum-mass solar nebula" and with nominal magnetorotational instability (MRI) turbulence, we find that accretion proceeds only for planetesimals with sizes above ~300 km at 1 AU and ~1000 km at 5 AU. We find that accretion is facilitated in disks with smaller masses. However, at 5 AU and for nominal turbulence strength, km-sized planetesimals are in a highly erosive regime even for a disk mass as small as a fraction of the mass of Jupiter. The existence of giant planets implies that either turbulence was weaker than calculated by standard MRI models or some mechanism was capable of producing Ceres-mass planetesimals on very short timescales. In any case, our results show that in the presence of turbulence planetesimal accretion is most difficult in massive disks and at large orbital distances.

Subject headings: accretion, accretion disks — planets and satellites: formation — solar system: formation — turbulence

Online material: color figures

1. INTRODUCTION

It is often considered that the evolution of protoplanetary disks and the consequent accretion of gas by the central protostar are driven by turbulent viscosity due to a magnetorotational instability (MRI; e.g., Balbus & Hawley 1991). Laughlin et al. (2004) and Nelson & Papaloizou (2004) carried out fluid dynamical simulations of MRI and found that the random torques due to the turbulent density fluctuations give rise to a random walk in the semimajor axes of planetesimals. Rice & Armitage (2003) pointed out through model calculations that the random walk expands the effective feeding zone of protoplanets and may lead to rapid formation of large cores for gas giants. Through a Fokker-Planck treatment, Johnson et al. (2006) also pointed out the importance of the random walk in planet accretion. Adopting the semianalytical formula for the random torque derived by Laughlin et al. (2004), Ogihara et al. (2007) performed *N*-body simulations for the late stages of terrestrial planet accretion with a disk significantly depleted in gas, starting from Mars-mass protoplanets. They found that the MRI turbulence indeed helps to reduce the number of accreted terrestrial planets which is otherwise too large compared to our solar system.

However, Nelson (2005) found through direct integrations of the orbits of protoplanets in a MRI turbulent disk that orbital eccentricities are also excited. Britsch et al. (2008) also found a similar feature in a self-gravitating disk. While the random walk itself is favorable to the growth of protoplanets by avoiding isolation, the excitation of their eccentricities, which had been neglected in Rice & Armitage (2003) and Johnson et al. (2006), is a threat for planetesimal accretion processes because of increased collision velocity. Unfortunately, Nelson's (2005) orbital integrations were limited to 100–150 Keplerian times and neglected collision processes, so that it is not possible to conclude from that work whether planetesimals should grow or be eroded in the presence of turbulence.

In the present article, we explore by which paths planetesimals may have grown to planet-sized bodies in turbulent disks. Because the level of density fluctuations due to the MRI turbulence is not well determined, we choose to study the qualitative effects of the turbulence on the accretion of planetesimals and their dependence on the key parameters of the problem, in particular the progressive removal of the gas disk. In § 2 we summarize the conditions for the accretion and destruction of planetesimals in terms of their orbital eccentricities. In § 3 we analytically derive the equilibrium eccentricity for which the excitation due to turbulence is balanced by damping due to tidal interactions with the disk gas, aerodynamic gas drag, and collisions. Comparing the equilibrium eccentricities with critical eccentricities for accretion and destruction, we derive critical physical radii and masses of planetesimals for accretion or destruction. The results are applied to viscously evolving disks (§ 4). We then discuss possible solutions for the problem of the formation of planetesimals and planets (§ 5).

2. ACCRETION AND DESTRUCTION CONDITIONS

We summarize the accretion and destruction conditions below. From energy conservation, the collision velocity ($v_{\rm coll}$) between two planetesimals (labeled 1 and 2) satisfies

$$E = \frac{1}{2} v_{\rm coll}^2 - \frac{G(M_1 + M_2)}{R_1 + R_2} = \frac{1}{2} v_{\rm rel}^2, \quad (1)$$

where M_j and R_j are the mass and physical radius of a planetesimal j ($j = 1, 2$), and $v_{\rm rel}$ is their relative velocity when they are apart

from each other. When the velocity dispersion of planetesimals $v_{\rm disp}$ is larger than the Hill velocity that is given by $(M/3M_*)^{1/3}v_{\rm K}$, where M_* is the mass of the host star and $v_{\rm K}$ is the Keplerian velocity, $v_{\rm rel}$ is approximated by $v_{\rm disp}$ (e.g., Ida & Nakazawa 1989; Ida 1990). The total energy then becomes

$$2E = v_{\rm coll}^2 - v_{\rm esc}^2 \simeq v_{\rm disp}^2, \tag{2}$$

where $v_{\rm esc}$ is the (two-body) surface escape velocity defined by

$$v_{\rm esc} = \sqrt{\frac{2G(M_1+M_2)}{R_1+R_2}}. \tag{3}$$

Collisional dissipation decreases the energy by some fraction of $v_{\rm coll}^2/2$. If $v_{\rm disp} \ll v_{\rm esc}$, the collisional dissipation results in $E<0$ after collision. On the other hand, E is likely to be still positive after a collision with $v_{\rm disp} \gg v_{\rm esc}$. Thus, for moderate dissipation, the condition for an accretional collision is $v_{\rm disp} < v_{\rm esc}$ (e.g., Ohtsuki 1993). Since the orbital eccentricity $e \simeq v_{\rm disp}/v_{\rm K}$, a collision should result in accretion for $e < e_{\rm acc}$, where

$$\begin{aligned} e_{\rm acc} \simeq \frac{v_{\rm esc}}{v_{\rm K}} &\simeq 0.28\left(\frac{M}{M_\oplus}\right)^{1/3}\left(\frac{\rho_p}{3\ {\rm g\ cm^{-3}}}\right)^{1/6}\left(\frac{r}{1\ {\rm AU}}\right)^{1/2} \\ &\simeq 0.036\left(\frac{R}{10^3\ {\rm km}}\right)\left(\frac{\rho_p}{3\ {\rm g\ cm^{-3}}}\right)^{1/2}\left(\frac{r}{1\ {\rm AU}}\right)^{1/2}. \end{aligned} \tag{4}$$

In the above relation, ρ_p is the bulk density of the planetesimals and $M \sim M_j$ (for simplicity, $M_1 \sim M_2$ is assumed). The physical radius R is given by

$$R = 7.8\times10^8 (M/M_\oplus)^{1/3}\left[\rho_p/\left(3\ {\rm g\ cm^{-3}}\right)\right]^{-1/3}\ {\rm cm}. \tag{5}$$

A collision results in destruction if the collision velocity is such that the specific kinetic energy of a collision ($v_{\rm coll}^2/2$) exceeds

$$Q_D \simeq \left[Q_0\left(\frac{R}{1\ {\rm cm}}\right)^a + 3B\left(\frac{\rho_p}{3\ {\rm g\ cm^{-3}}}\right)\left(\frac{R}{1\ {\rm cm}}\right)^b\right]{\rm erg\ g^{-1}}, \tag{6}$$

where Q_0 is the material strength, $B \simeq 0.3$–2.1, $a \simeq -0.4$, and $b \simeq 1.3$ (Benz & Asphaug 1999). For basalt rocks or water ice, $Q_0 \simeq 10^7$–10^8 (Benz & Asphaug 1999), but it can take a significantly smaller value for loose aggregates.[1]

We adopt $Q_0 = 3\times10^7$ as a nominal value. Self-gravity (the second term on the right-hand side) dominates the material strength when $R \gtrsim 100$ m. In this regime, adopting $B \sim 1$, a collision results in destruction for $e > e_{\rm dis}$, where

$$\begin{aligned} e_{\rm dis} \simeq \frac{\sqrt{2Q_D}}{v_{\rm K}} &\simeq 0.50\left(\frac{M}{M_\oplus}\right)^{0.22}\left(\frac{\rho_p}{3\ {\rm g\ cm^{-3}}}\right)^{0.28}\left(\frac{r}{1\ {\rm AU}}\right)^{1/2} \\ &\simeq 0.13\left(\frac{R}{10^3\ {\rm km}}\right)^{0.65}\left(\frac{\rho_p}{3\ {\rm g\ cm^{-3}}}\right)^{0.5}\left(\frac{r}{1\ {\rm AU}}\right)^{1/2}. \end{aligned} \tag{7}$$

3. EQUILIBRIUM ECCENTRICITIES

We first derive the equilibrium eccentricities of planetesimals at which the excitation by the MRI turbulence is balanced by damping due to drag and/or collisions. Comparing the estimated eccentricities with $e_{\rm acc}$ and $e_{\rm dis}$, we then evaluate the outcome of collisions between planetesimals as a function of planetesimal size, turbulence strength, and surface density of disk gas.

For an easy interpretation, we provide in this section analytical relations based on a model in which the gas and solid components of disk surface density are scaled with the multiplicative factors f_g and f_d,

$$\Sigma_g = 2400 f_g\left(\frac{r}{1\ {\rm AU}}\right)^{-3/2}\ {\rm g\ cm^{-2}}, \tag{8}$$

$$\Sigma_d = 10 f_d\,\eta_{\rm ice}\left(\frac{r}{1\ {\rm AU}}\right)^{-3/2}\ {\rm g\ cm^{-2}}, \tag{9}$$

where $\eta_{\rm ice} \simeq 3$–4 is an enhancement factor of Σ_d due to ice condensation. If $f_g = f_d = 1$, Σ_g and Σ_d are 1.4 times those of the minimum-mass solar nebula model (Hayashi 1981).

In this section we also use the disk temperature distribution obtained in the optically thin limit (Hayashi 1981),

$$T \simeq 280\left(\frac{r}{1\ {\rm AU}}\right)^{-1/2}\left(\frac{L_*}{L_\odot}\right)^{1/4}\ {\rm K}, \tag{10}$$

where L_* and $L_\odot$ are the stellar and solar luminosities, respectively. The corresponding sound velocity is

$$c_s = 1.1\times10^5\left(\frac{r}{1\ {\rm AU}}\right)^{-1/4}\left(\frac{L_*}{L_\odot}\right)^{1/8}\ {\rm cm\ s^{-1}}. \tag{11}$$

Since the disk scale height is given by $h = \sqrt{2}c_s/\Omega_{\rm K}$ (assuming that T is vertically uniform in the disk), equations (8) and (11) yield the disk gas density at the midplane as

$$\rho_g = \frac{\Sigma_g}{\sqrt{\pi}h} = 2\times10^{-9} f_g\left(\frac{r}{1\ {\rm AU}}\right)^{-11/4}\ {\rm g\ cm^{-3}}. \tag{12}$$

3.1. *Excitation*

The orbital eccentricities of planetesimals are pumped up both by the random gravitational perturbations from density fluctuations of disk gas, as well as by mutual gravitational scattering among planetesimals. Assuming planetesimals have equal masses, their orbital eccentricities should be excited to at most $\sim e_{\rm acc}$ by the mutual scattering (e.g., Safronov 1969). As is shown below, the value of this eccentricity is smaller than that due to the turbulent excitation, except for very large planetesimals ($\sim 10^3$ km or larger), and/or in the case of significantly depleted gas disks. For simplicity, in this work we choose to neglect the possibility that mutual scattering dominates over turbulent excitation. It is therefore important to note that our results may be slightly optimistic when concerning the possibility of accretion of massive planetesimals.

The orbital eccentricities that result from the turbulent density fluctuations in the disk are provided by Ogihara et al. (2007), on the basis of orbital integrations with empirical formula by Laughlin et al. (2004), as

$$\begin{aligned} e &\sim 0.1\gamma\left(\frac{\Sigma_g}{\Sigma_{g,1}}\right)\left(\frac{r}{1\ {\rm AU}}\right)^2\left(\frac{t}{T_{\rm K}}\right)^{1/2} \\ &= 0.1 f_g\gamma\left(\frac{r}{1\ {\rm AU}}\right)^{-1/4}\left(\frac{t}{1\ {\rm yr}}\right)^{1/2}, \end{aligned} \tag{13}$$

[1] For porous materials, Q_0 is rather higher (W. Benz 2008, private communication).

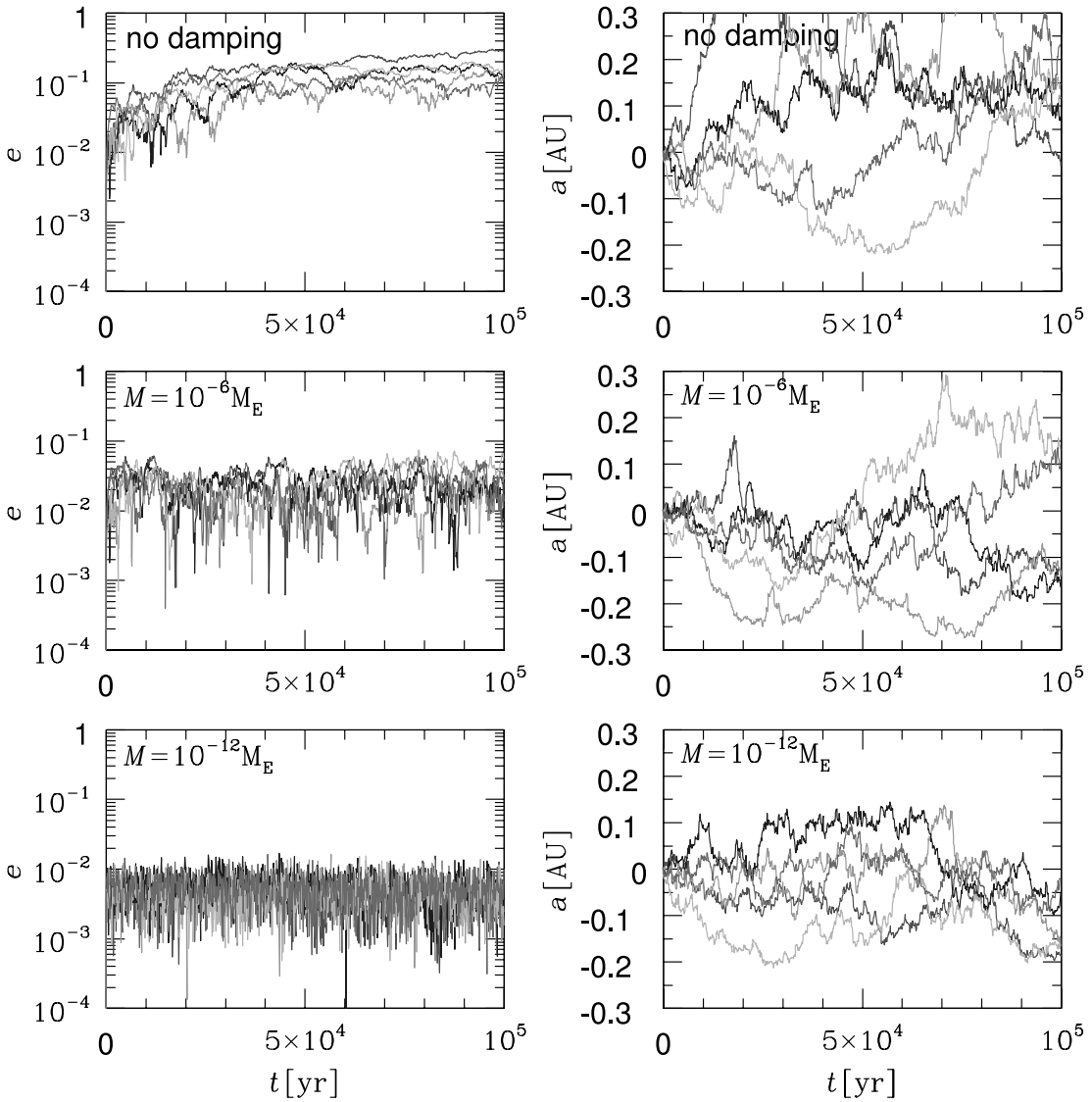

FIG. 1.—Evolution of the eccentricity (*left*) and of the semimajor axis (*right*) as a function of time, for different planetesimal masses (top to bottom). A single planetesimal is integrated in a turbulent disk, and five independent runs with different random number seeds for the generation of turbulent density fluctuations are shown in each panel. *Top*: We consider no tidal and gas drag. *Middle*: Results including gas drag for planetesimals of $M = 10^{-6}\ M_\oplus$. *Bottom*: Results for planetesimals of $M = 10^{-12}\ M_\oplus$. In all cases, we assume an initial orbital distance of 1 AU, $f_g = 1$, and $\gamma = 0.01$. [*See the electronic edition of the Journal for a color version of this figure.*]

where $\Sigma_{g,1}$ is Σ_g at 1 AU with $f_g = 1$ (eq. [8]) and γ is a nondimensional parameter used to express the disk turbulence.[2] Although Ogihara et al. (2007) showed the results only at $\sim$1 AU, we here added a dependence on r using scaling arguments (see the Appendix). Orbital integrations for other r show a consistent dependence. Note that $\Delta a/a \sim e$, where Δa is the amplitude of random walk in semimajor axis. Since $e \ll 1$, the radial distance r and semimajor axis a are identified here.

[2] Although Ogihara et al. (2007) suggested that eq. (13) may be enhanced by a factor 10 by the inclusion of $m = 1$ modes, the $m = 1$ modes actually enhance only the amplitude of random walk in semimajor axis (Δa) but not the eccentricity. Since higher m modes fluctuate over shorter timescales, they tend to cancel out on the orbital period of a planetesimal. For these modes, $\Delta a/a$, which is due to time variation of the potential, is much smaller than Δe, because the latter is also excited by the nonaxisymmetric structure. The inclusion of slowly varying $m = 1$ modes enhances $\Delta a/a$ up to the order of $\sim e$. On the other hand, the definition of Γ in eqs. (5) and (34) of Ogihara et al. (2007) should be multiplied by π. We use eq. (13) for the eccentricity excitation, which is consistent with an orbital calculation including $m = 1$ modes (Fig. 1).

From the simulation results by Laughlin et al. (2004), the value of γ may be $\sim(1/3)(\delta\rho/\rho) \sim 10^{-3}$ to 10^{-2} for MRI turbulence. In this paper, we use $\gamma = 10^{-3}$ as a fiducial value. Interestingly, with a quite different approach, Johnson et al. (2006) derived a similar formula for $\Delta a/a$ with the same dependences on r, Σ_g, and t. If $e \simeq \Delta a/a$, their formula is consistent with ours. They suggested that $\gamma \sim \alpha$ or $\alpha^{1/2} h/a$, where h is disk scale height and α is the parameter for the α-prescription for turbulent viscosity (Shakura & Sunyaev 1973). For $\alpha \sim 10^{-3}$ to 10^{-2}, their estimate is also similar to our fiducial value.

The top panels in Figure 1 show the results of an orbital integration with a fourth-order Hermite scheme for the evolution of e and $\Delta a/a$ with turbulent perturbations but without any damping. Five independent runs with different random number seeds for the generation of turbulent density fluctuations (Ogihara et al. 2007) are plotted in each panel. The initial e and i are 10^{-6}. For $f_g = 1, \gamma = 0.01$, and $r = 1$ AU, as used in Figure 1, equation (13) is reduced to $e \sim 10^{-3}(t/1\ \mathrm{yr})^{1/2}$. To highlight the effect of turbulence, we used a larger value of γ than the fiducial value. The

evolution of the rms's of the five runs in Figure 1 agrees with equation (13) within a factor of ~2. From equation (13), the excitation timescale is

$$\tau_{\rm exc} = \frac{e}{de/dt} \simeq 2\times10^2\gamma^{-2}e^2\left(\frac{\Sigma_g}{\Sigma_{g,1}}\right)^{-2}\left(\frac{r}{1\ {\rm AU}}\right)^{-4}T_{\rm K} = 2\times10^2 f_g^{-2}\gamma^{-2}e^2\left(\frac{r}{1\ {\rm AU}}\right)^{1/2}\ {\rm yr}. \quad (14)$$

3.2. *Damping*

The eccentricity-damping processes are (1) tidal interaction with disk gas, (2) aerodynamical gas drag, and (3) inelastic collisions. The tidal damping timescale 1 is derived by Tanaka & Ward (2004) as

$$\tau_{\rm tidal} \simeq 1.3\left(\frac{M}{M_\odot}\right)^{-1}\left(\frac{\Sigma_g r^2}{M_\odot}\right)^{-1}\left(\frac{c_s}{v_{\rm K}}\right)^4\Omega_{\rm K}^{-1} \simeq 3\times10^2 f_g^{-1}\left(\frac{M}{M_\oplus}\right)^{-1}\left(\frac{r}{1\ {\rm AU}}\right)^2\ {\rm yr}. \quad (15)$$

The gas drag damping timescale 2 is derived by Adachi et al. (1976) as

$$\tau_{\rm drag} \simeq \frac{Mv_{\rm disp}}{\pi R^2\rho_g v_{\rm disp}^2} \simeq 2\times10^4 f_g^{-1}e^{-1}\left(\frac{M}{M_\oplus}\right)^{1/3}\left(\frac{\rho_p}{3\ {\rm g\ cm^{-3}}}\right)^{2/3}\left(\frac{r}{1\ {\rm AU}}\right)^{13/4}\ {\rm yr}. \quad (16)$$

For simplicity, we evaluate the damping timescale due to inelastic collision as the mean collision time of planetesimals, assuming that all the planetesimals have the same mass M. Since in the size distribution caused by collision cascade, collisions with comparable-sized bodies and those with smaller ones contribute similarly, the neglection of the size distribution may not be too problematic. Since we look for the conditions in which collisions are nonaccretional, we consider the case with $v_{\rm disp} > v_{\rm esc}$. Assuming that the gravitational focusing factor $[1 + (v_{\rm esc}/v_{\rm disp})^2] \sim 1$, the collision damping timescale is

$$\tau_{\rm coll} \simeq \frac{1}{n\pi R^2 v_{\rm disp}} \simeq 2\times10^7 f_d^{-1}\eta_{\rm ice}^{-1}\left(\frac{M}{M_\oplus}\right)^{1/3}\left(\frac{\rho_p}{3\ {\rm g\ cm^{-3}}}\right)^{2/3}\left(\frac{r}{1\ {\rm AU}}\right)^3{\rm yr}, \quad (17)$$

where n is the spatial number density of planetesimals. Note that $n \sim (\Sigma_d/M)/(v_{\rm disp}/\Omega_{\rm K})$.

3.3. *Equilibrium Eccentricity*

We now equate equation (14) with equations (15), (16), and (17), respectively, to obtain an equilibrium eccentricity for each damping process. For simplicity and to a good approximation, the actual equilibrium eccentricity can be approximated as the minimum of the three equilibrium eccentricities. From equations (14) and (15),

$$e_{\rm tidal} \simeq 1.2 f_g^{1/2}\gamma\left(\frac{M}{M_\oplus}\right)^{-1/2}\left(\frac{r}{1\ {\rm AU}}\right)^{3/4} \simeq 24 f_g^{1/2}\gamma\left(\frac{R}{10^3\ {\rm km}}\right)^{-3/2}\left(\frac{\rho_p}{3\ {\rm g\ cm^{-3}}}\right)^{-1/2}\left(\frac{r}{1\ {\rm AU}}\right)^{3/4}. \quad (18)$$

With equation (16),

$$e_{\rm drag} \simeq 4.6 f_g^{1/3}\gamma^{2/3}\left(\frac{M}{M_\oplus}\right)^{1/9}\left(\frac{\rho_p}{3\ {\rm g\ cm^{-3}}}\right)^{2/9}\left(\frac{r}{1\ {\rm AU}}\right)^{11/12} \simeq 0.23 f_g^{1/3}\gamma^{2/3}\left(\frac{R}{1\ {\rm km}}\right)^{1/3}\left(\frac{\rho_p}{3\ {\rm g\ cm^{-3}}}\right)^{1/3}\left(\frac{r}{1\ {\rm AU}}\right)^{11/12}. \quad (19)$$

For $f_g = 1$, $\gamma = 0.01$, and $r = 1$ AU, equation (19) predicts that $e_{\rm drag} \simeq 0.045$ for $M/M_\oplus = 10^{-6}$ and $e_{\rm drag} \simeq 0.01$ for $M/M_\oplus = 10^{-12}$. An orbital integration in the middle and bottom panels in Figure 1 shows that the results agree with the analytical estimate within a factor ~1.5. With equation (17),

$$e_{\rm coll} \simeq 3.2\times10^2 f_g(f_d\eta_{\rm ice})^{-1/2}\gamma\times\left(\frac{M}{M_\oplus}\right)^{1/6}\left(\frac{\rho_p}{3\ {\rm g\ cm^{-3}}}\right)^{1/3}\left(\frac{r}{1\ {\rm AU}}\right)^{5/4} \simeq 3.6 f_g(f_d\eta_{\rm ice})^{-1/2}\gamma\times\left(\frac{R}{1\ {\rm km}}\right)^{1/2}\left(\frac{\rho_p}{3\ {\rm g\ cm^{-3}}}\right)^{5/6}\left(\frac{r}{1\ {\rm AU}}\right)^{5/4}. \quad (20)$$

In Figure 2, the equilibrium eccentricity, $e_{\rm eq} = \min(e_{\rm tidal}, e_{\rm drag}, e_{\rm coll})$, is plotted with solid curves as a function of the planetesimal radius R, the corresponding planetesimal mass being $M = 2.1\times10^{-3}(R/10^3\ {\rm km})^3(\rho_p/3\ {\rm g\ cm^{-3}})M_\oplus$, Note again that the effect of mutual planetesimal scattering is neglected. For bodies with more than Lunar to Martian masses, tidal damping is dominant. This yields a decrease in the equilibrium eccentricity with increasing planetesimal radius for $R \gtrsim 100$ km. For smaller mass bodies, gas drag damping dominates tidal damping and the equilibrium eccentricity increases with increasing R. For the smallest planetesimal sizes (the regions with the slightly steeper positive gradient), collision damping is dominant, but with a significant contribution of gas drag damping.

The limiting mass and radius at which $e_{\rm drag}$ (eq. [19]) and $e_{\rm acc}$ (eq. [4]) cross are

$$M_{\rm acc} \simeq 3.0\times10^{-4} f_g^{3/2}\left(\frac{\gamma}{10^{-3}}\right)^3\times\left(\frac{\rho_p}{3\ {\rm g\ cm^{-3}}}\right)^{-1/4}\left(\frac{r}{1\ {\rm AU}}\right)^{9/8}M_\oplus,$$
$$R_{\rm acc} \simeq 5.2\times10^2 f_g^{1/2}\left(\frac{\gamma}{10^{-3}}\right)\times\left(\frac{\rho_p}{3\ {\rm g\ cm^{-3}}}\right)^{-5/12}\left(\frac{r}{1\ {\rm AU}}\right)^{3/8}\ {\rm km}. \quad (21)$$

The accretion of planetesimals is possible for $M > M_{\rm acc}$ ($R > R_{\rm acc}$). In the top panel of Figure 2 ($\gamma = 10^{-3}$ and $f_g = 1$), planetesimal accretion proceeds in a range of R values in which the solid curve ($e_{\rm eq}$) is located below the dashed curve ($e_{\rm acc}$), that is, only if a body is larger than Ceres. Such large planetesimals can be formed by a different mechanism than pairwise accretion such as self-gravitational instability in turbulent eddies (e.g., Johansen et al. 2007; Cuzzi et al. 2008). When the disk gas is removed, accretion becomes possible for smaller planetesimals (the second panel of Fig. 2). On the other hand, if turbulence is stronger ($\gamma \sim 10^{-2}$), planetesimal accretion requires more than 1000 km-sized bodies. This appears to be an insurmountable barrier to accretion, even for

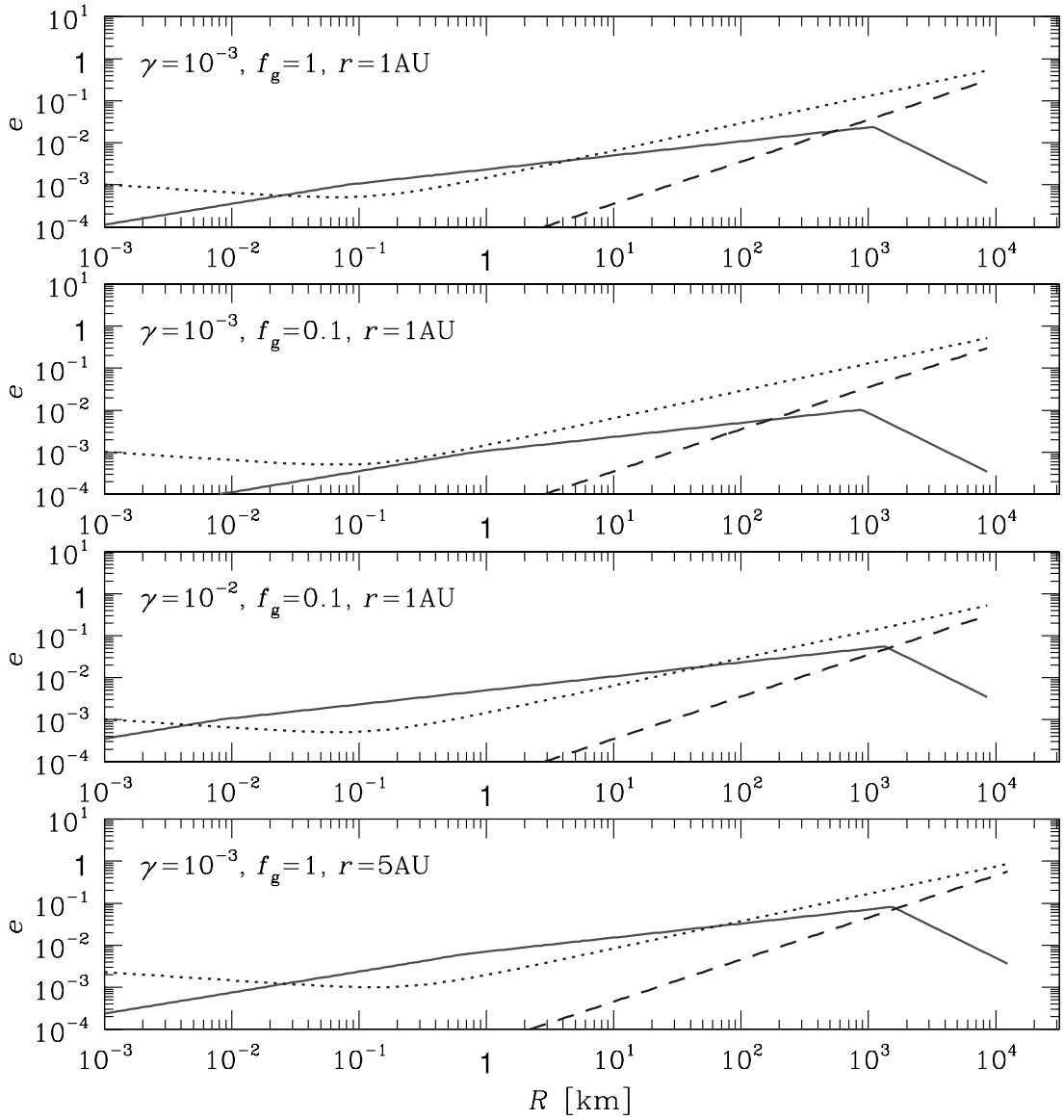

FIG. 2.—Equilibrium eccentricities ($e_{\rm eq}$) as a function of the physical radius R of planetesimals (*solid curves*). The value of $e_{\rm eq}$ is determined by the minimum of individual equilibrium eccentricities, $e_{\rm tidal}$, $e_{\rm drag}$, and $e_{\rm coll}$. The critical values for accretion and destruction, $e_{\rm acc}$ and $e_{\rm dis}$, are also plotted by dashed and dotted curves, respectively. At $r = 1$ AU, the bulk density $\rho_p = 3$ g cm $^{-3}$ is assumed, while $\rho_p = 1$ g cm $^{-3}$ at 5 AU. The mass of the planetesimals is given by $M = 2.1 \times 10^{-3}(R/10^3\ {\rm km})^3(\rho_p/3\ {\rm g\ cm^{-3}})\ M_\oplus$. [*See the electronic edition of the Journal for a color version of this figure.*]

depleted gaseous disks ($f_g \sim 0.1$), as shown in the third panel of Figure 2. Finally, at large orbital radii, planetesimal accretion is even more difficult (Fig. 2, *bottom*).

Another critical mass (radius) is the point at which $e_{\rm drag}$ (eq. [19]) and $e_{\rm dis}$ in the gravity regime (eq. [7]) cross,

$$M_{\rm dis} \simeq 6 \times 10^{-11} f_g^{3.3} \left(\frac{\gamma}{10^{-3}}\right)^{6.7} \times \left(\frac{\rho_p}{3\ {\rm g\ cm^{-3}}}\right)^{-0.6} \left(\frac{r}{1\ {\rm AU}}\right)^{4.2} M_\oplus,$$

$$R_{\rm dis} \simeq 3 f_g^{1.1} \left(\frac{\gamma}{10^{-3}}\right)^{2.2} \left(\frac{\rho_p}{3\ {\rm g\ cm^{-3}}}\right)^{-0.53} \left(\frac{r}{1\ {\rm AU}}\right)^{1.4} {\rm km}. \quad (22)$$

Planetesimals with $M < M_{\rm dis}$ ($R < R_{\rm dis}$) are disrupted by collisions down to the sizes for which material strength is dominant (see below). For $\gamma \sim 10^{-3}$ and $f_g \sim 1$ (the top panel of Fig. 2), planetesimals with sizes larger than several km in radius survive but without growing, while smaller planetesimals are disrupted.

When a planetesimal is smaller than ~100 m in size, it is bounded by material strength rather than self-gravity. In the regime of material strength, $Q_D \sim Q_0(R/1\ {\rm cm})^{-0.4}$. The body is not disrupted if $(2Q_D)^{1/2}/v_{\rm K} > e_{\rm drag}$, which is equivalent to

$$M \lesssim M_{\rm mat} \simeq 0.8 \times 10^{-17} f_g^{-1.9} \left(\frac{\gamma}{10^{-3}}\right)^{-3.7} \times \left(\frac{\rho_p}{3\ {\rm g\ cm^{-3}}}\right)^{-0.9} \left(\frac{r}{1\ {\rm AU}}\right)^{2.8} M_\oplus,$$

$$R \lesssim R_{\rm mat} \simeq 16 f_g^{-0.62} \left(\frac{\gamma}{10^{-3}}\right)^{-1.25} \times \left(\frac{\rho_p}{3\ {\rm g\ cm^{-3}}}\right)^{-0.62} \left(\frac{r}{1\ {\rm AU}}\right)^{2.8} {\rm m}. \quad (23)$$

Since in this regime, collision damping is slightly stronger than gas drag, actual values of $M_{\rm mat}$ and $R_{\rm mat}$ are determined by $(2Q_D)^{1/2}/v_{\rm K} > e_{\rm coll}$, so they are slightly larger than the above

estimate (see Fig. 2). When $\tau_{\rm drag}\Omega_{\rm K} \lesssim 1$, the planetesimals' motions are coupled to that of the gas. The collision velocity then cannot be expressed in terms of orbital eccentricity. This limiting size is however much smaller than $R_{\rm mat}$. The collision cascade would hence stop at $M \sim M_{\rm mat}$ ($R \sim R_{\rm mat}$). Regions for which the dotted curves ($e_{\rm dis}$) in Figure 2 have negative gradients correspond to the material strength regime. In the depleted disk case, $e_{\rm dis}$ is always larger than $e_{\rm eq}$, so that the disruptive regions do not exist (see the second panel of Fig. 2). Note that $R_{\rm mat} \propto Q_0^{0.94}$. If the planetesimals are loose aggregates so that $Q_0 < 3 \times 10^7$ (the value for basalt rocks or water ice), the limiting size $R_{\rm mat}$ is smaller.

4. ACCRETION/DESTRUCTION OF PLANETESIMALS IN AN EVOLVING DISK

We now put these various critical physical radii in the context of the evolution of the protoplanetary disk. In order to investigate the effect of departures from power-law relations of the surface density and temperature profiles in real disks, we also present in this section results obtained from a one-dimensional disk model that includes an α-viscosity and photoevaporation (see Guillot & Hueso 2006; Hueso & Guillot 2005). The parameters used in the model presented here are a turbulent viscosity $\alpha = 0.01$ and an evaporation parameter $T_{\rm atm} = 100$ K (the temperature of the evaporation part of the outer disk). Another choice of the parameters would affect the results only marginally.

In the numerical calculation in this section, we evaluate the equilibrium eccentricities $e_{\rm eq}$ as a function of planetesimal radius by solving the following relation,

$$\tau_{\rm exc}^{-1} = \tau_{\rm tidal}^{-1} + \tau_{\rm drag}^{-1} + \tau_{\rm coll}^{-1}, \quad (24)$$

where the different timescales are given by equations (14)–(17). The survival physical radius for accretion $R_{\rm acc}$ is then found, for each orbital radius in the protoplanetary disk and for each time step, by solving the equation

$$e_{\rm eq}(R_{\rm acc}) = e_{\rm acc}(R_{\rm acc}), \quad (25)$$

where $e_{\rm acc}$ is given by equation (4). When the mean kinetic energy is larger than the strength of a planetesimal, the collision is highly erosive. We then obtain the range $R < R_{\rm dis}$ corresponding to the highly erosive collisions by solving the equation

$$e_{\rm eq}(R_{\rm dis}) = \frac{\sqrt{2Q_D(R_{\rm dis})}}{v_{\rm K}}, \quad (26)$$

where Q_D is given by equation (6).

Figures 3–5 show our results for three values of the turbulent excitation parameter, $\gamma = 10^{-2}$, 10^{-3} (our fiducial value), and 10^{-4}. Each figure shows, for three orbital distances, 1, 5, and 30 AU, the planetesimal physical radii corresponding to accretive and erosive regions plotted as a function of the total mass remaining in the disk. Since the disk mass decreases with time as a result of viscous evolution and photoevaporation, a decrease in disk mass corresponds to evolution in time. As shown in § 3, planetesimal accretion becomes easier as the disk becomes less massive simply because the turbulent excitation, directly proportional to the local surface density of the gas, becomes weaker. However, after some point, the disk becomes too light to provide a sufficient amount of gas to form Jupiter-mass gas giants.

The figures also show as thin black curves the values obtained for a disk that follows the slope in surface density versus orbital distance defined for the minimum-mass solar nebula (eq. [8]) as a function of disk mass. The disk mass in this model is given by

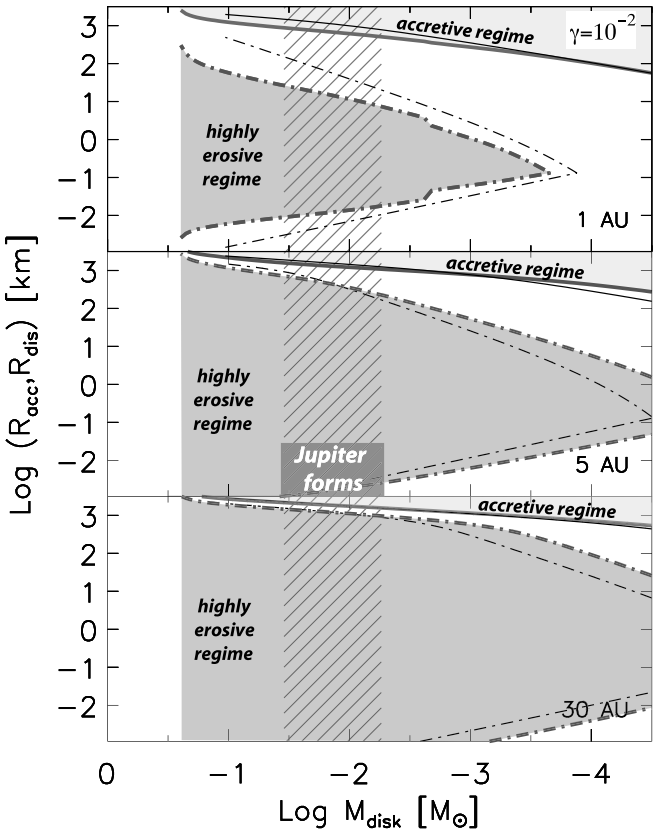

FIG. 3.—Evolution of characteristic physical radii of planetesimals as a function of disk mass, at several orbital distances in the disk, 1 (*top*), 5 (*middle*), and 30 AU (*bottom*). The solid and dot-dashed curves correspond to the boundary radius for the accretion regime ($R_{\rm acc}$) and to that of the highly erosive regime ($R_{\rm dis}$). Two disk models have been used: a simple power-law model with $d \ln \Sigma_g / d \ln r = -3/2$ (eq. [8]) with an outer cutoff radius of 1000 AU (*thin curves*), and an α-disk model with $\alpha = 0.01$ and $T_{\rm atm} = 100$ K (*thick curves*; see Guillot & Hueso 2006). The hatched region corresponds to the range of disk mass (equivalently, the range of time if disk evolution is given) during which Jupiter must start accreting hydrogen/helium gas (assuming it grabs between 10% and 70% of the disk mass flux at its orbital distance). In the simulations, MRI turbulence is supposed to be high, with $\gamma = 10^{-2}$. We also choose $Q_0 = 3 \times 10^7$ and $B = 1$ (see eq. [6]). [*See the electronic edition of the Journal for a color version of this figure.*]

$3.4 \times 10^{-2} f_g (r_{\rm edge}/100\ {\rm AU})^{1/2}\ M_\odot$, where $r_{\rm edge}$ is the outer edge radius of the disk. Although the original minimum-mass solar nebula model by Hayashi (1981) used $r_{\rm edge} = 35$ AU, we here adopt $r_{\rm edge} = 1000$ AU (for comparison, our fiducial α-disk model with $T_{\rm atm} = 100$ K extends up to a maximum of 350 AU).

These are found to be in excellent agreement with the analytical expressions derived in § 3, with small differences arising from the simplifications inherent to the analytical approach. Larger differences are found between the power-law disk and the α-disk models mostly because of the difference in slopes ($d \ln \Sigma / d \ln r = -3/2$ for the former, ~ -1 for the α-disk) which implies that a given disk mass does not correspond to the same surface density with two models, the difference being larger at smaller orbital distances. However, the qualitative features of accretive and erosive regions are similar to each other. It should be noted that the models also differ in their temperature profiles, but this is found to be less important.

In the highly turbulent regime presented in Figure 3, a self-sustained regime of accretion becomes possible only when planetesimals have become very large/massive, with sizes generally well over 100 km. This case also yields a sustained area of high erosion where the average kinetic energies of planetesimals are

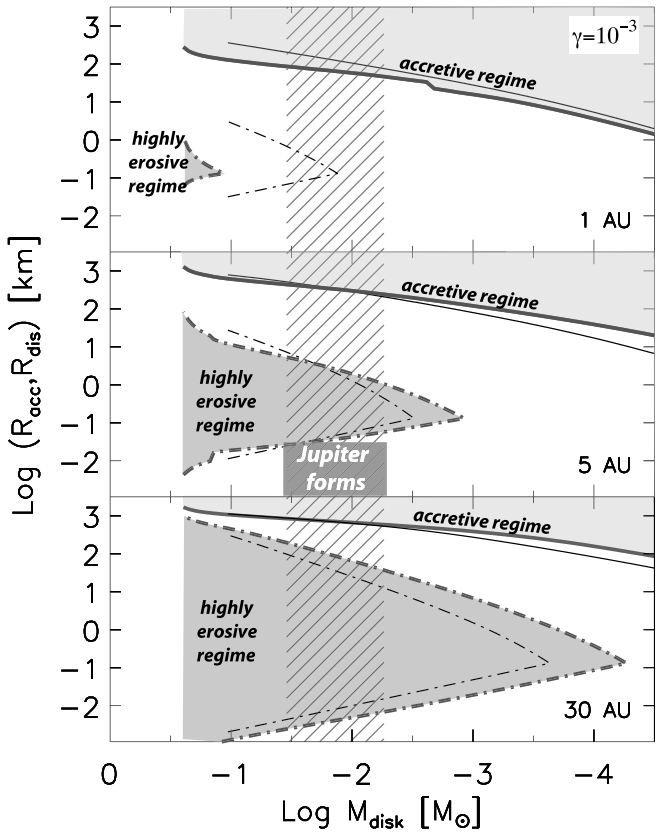

FIG. 4.—Same as Fig. 3, but for a medium turbulence case ($\gamma = 10^{-3}$; our fiducial case). [*See the electronic edition of the Journal for a color version of this figure.*]

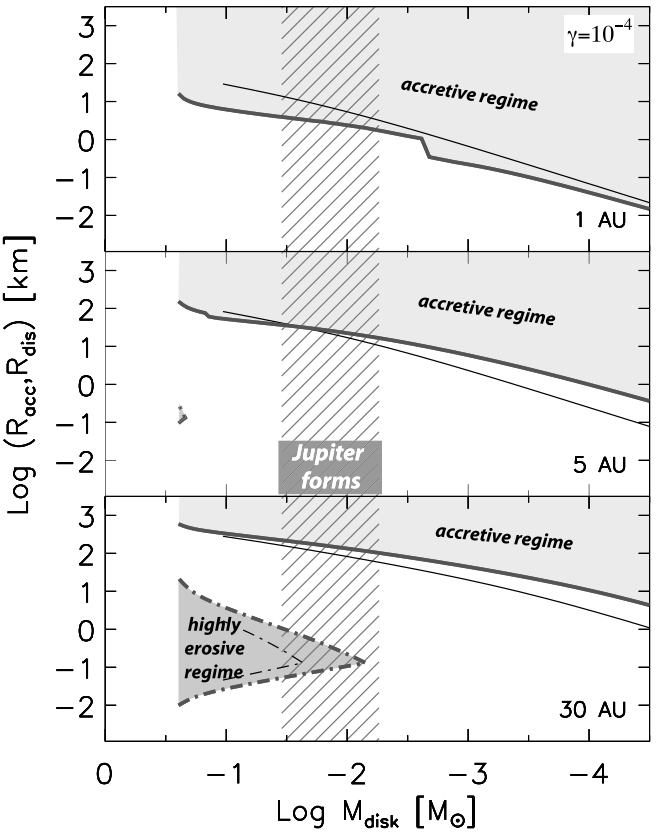

FIG. 5.—Same as Fig. 3, but for a weak turbulence case ($\gamma = 10^{-4}$). [*See the electronic edition of the Journal for a color version of this figure.*]

above their internal energies. It is difficult to imagine how planetary cores can form in this context especially if they have to grow large enough to form giant planets.

With smaller perturbations from the turbulent disk (Fig. 4), planetesimals have more possibilities to accrete; with time, as the disk mass decreases, the inner disk rapidly moves out of the highly erosive regime, while erosion still remains important at large orbital distances. With a turbulence strength parameter $\gamma = 10^{-4}$, corresponding to a very weak turbulence (Fig. 5), the presence of a highly erosive regime centered around $\sim$300 m planetesimals is limited only to the outer regions ($\gtrsim$30 AU), and the zone rapidly shrinks as the circumstellar gaseous disk disappears.

In order to put these findings into context, we also show the mass of the disk when Jupiter is believed to have started accreting its gaseous envelope. These values are calculated by assuming that the planet growth has been limited mostly by viscous diffusion in the disk, with the protoplanet capturing between 10% and 70% of the mass flux at its orbital distance in the disk evolution model by Hueso & Guillot (2005; for details, see Guillot & Hueso 2006). If giant planets have to form, at some time corresponding to the disk mass interval defined by the hatched areas in Figures 3–5, protoplanetary cores must be already large enough to start accreting the surrounding hydrogen and helium gas.

We can now define three important disk masses and their corresponding disk ages (with the warning that ages are inherently model dependent and are provided here for illustrative purposes only, on the basis of our particular model of α-disk evolution with photoevaporation):

1. The maximum mass of the disk, following the collapse of the molecular cloud. This mass can vary quite significantly from one disk formation/evolution model to another. For the particular model shown here, it is of the order of 0.25 $M_\odot$, for an age of 0.6 Myr.

2. The disk mass necessary for Jupiter to grow to its present mass if it captures 10% of the mass flux at its orbital distance. For realistic disk models, this depends weakly on parameters such as α and the disk evaporation rate. In our case, it corresponds to $M_{\rm disk} = 0.035\ M_\odot$ and an age of 1.95 Myr.

3. The disk mass necessary for Jupiter to grow to its present mass if it captures 70% of the mass flux at its orbital distance. For our model, $M_{\rm disk} = 0.0054\ M_\odot$ (about 5 times the mass of Jupiter) and an age of 2.85 Myr.

Table 1 provides the values of the physical radii that define the accretive regime and the highly erosive (disruptive) regime of Figures 3–5, namely, $R_{\rm acc}$ and $R_{\rm dis}$. In our solar system, the existence of Jupiter implies that either turbulence was low, the planet grew from a protoplanetary core formed in the inner solar system, or a mechanism was able to lead to the rapid formation of embryos larger than 240 km in radius at 5 AU (17 km in the low-turbulence case, 1080 km in the high-turbulence case) by the time when the disk mass had decreased to $5 \times 10^{-3}\ M_\odot$. In the last case, it appears that a mechanism such as the standard gravitational instability (e.g., Safronov 1969; Goldreich & Ward 1973) would not work because of the turbulence, but formation of relatively large protoplanets in eddies or vortexes (e.g., Johansen et al. 2007; Cuzzi et al. 2008; Barge & Someria 1995) is a promising possibility.

5. CONCLUSION AND DISCUSSION

We have investigated the critical physical radii for collisions between planetesimals to be accretional ($R > R_{\rm acc}$) or disruptive ($R < R_{\rm dis}$) in turbulent disks, as functions of turbulent strength

TABLE 1

LIMITS OF THE ACCRETIVE REGIME ($R > R_{acc}$) AND THE HIGHLY EROSIVE (DISRUPTIVE) REGIME (R_{dis}), AS A FUNCTION OF ORBITAL DISTANCE AND DISK MASS

	1 AU		5 AU		30 AU	
M_{disk} ($M_\odot$)	R_{acc} (km)	R_{dis} (km)	R_{acc} (km)	R_{dis} (km)	R_{acc} (km)	R_{dis} (km)
Fiducial: $\gamma = 10^{-3}$, $\rho_p = 3$ g cm^{-3}, $Q_0 = 3 \times 10^7$, $B = 1.0$						
0.25	280	[1.14, 0.061]	1280	[82, 0.00047]	1680	[1000, 0.00047]
0.035	86	...	440	[5.3, 0.026]	850	[200, 0.0024]
0.0054	46	...	240	[1.05, 0.057]	590	[37, 0.0069]
Low turbulence: $\gamma = 10^{-4}$, $\rho_p = 3$ g cm^{-3}, $Q_0 = 3 \times 10^7$, $B = 1.0$						
0.25	16	...	150	[0.30, 0.0099]	590	[22, 0.0099]
0.035	3.9	...	36	...	220	[1.07, 0.053]
0.0054	1.7	...	17	...	103	...
High turbulence: $\gamma = 10^{-2}$, $\rho_p = 3$ g cm^{-3}, $Q_0 = 3 \times 10^7$, $B = 1.0$						
0.25	2540	[300, 0.0026]	3920	[2770, 2×10^{-5}]	4250	[3220, 2×10^{-5}]
0.035	870	[26, 0.0090]	1590	[710, 0.0012]	2180	[1460, 0.00012]
0.0054	510	[7.4, 0.018]	1080	[230, 0.0025]	1580	[970, 0.00033]
High material resistance: $\gamma = 10^{-3}$, $\rho_p = 3$ g cm^{-3}, $Q_0 = 10^8$, $B = 2.0$						
0.25	280	[0.26, 0.15]	1280	[27, 0.0013]	1680	[700, 0.0013]
0.035	86	...	440	[1.6, 0.068]	850	[66, 0.0068]
0.0054	46	...	240	[0.27, 0.15]	590	[12, 0.019]
Low material resistance: $\gamma = 10^{-3}$, $\rho_p = 3$ g cm^{-3}, $Q_0 = 10^7$, $B = 0.3$						
0.25	280	[11, 0.026]	1280	[550, 0.00018]	1680	[1440, 0.00018]
0.035	86	[0.56, 0.087]	440	[41, 0.011]	850	[590, 0.00097]
0.0054	46	...	240	[9.2, 0.024]	590	[240, 0.0028]

NOTE.—The disruptive regime is the range in physical radii between the upper and lower limits (the left and right values) in the brackets.

[$\gamma \sim O(\Delta\rho/\rho)$], disk gas surface density, and orbital radius. The results presented here highlight the fact that MRI turbulence poses a great problem for the growth of planetesimals; generally, only those with sizes larger than a few hundred km are in a clearly accretive regime for a nominal value of $\gamma \sim 10^{-3}$. The others generally collide with velocities greater than their own surface escape velocities. For some of them, more severely in the km-size regime, collisions are likely to be disruptive. The problem is greater when the disk is still massive and at large orbital distances. Also, if turbulence is stronger than $\gamma \sim 10^{-2}$, planetesimal accretion becomes extremely difficult.

However, the rate of occurrence of extrasolar giant planets around solar-type stars is inferred to be as large as ~20% (Cumming et al. 2008) and depends steeply on the metallicity of the host star (Fischer & Valenti 2005; Santos et al. 2004). This strongly suggests that the majority of extrasolar giant planets were formed by core accretion followed by gas accretion onto the cores (Ida & Lin 2005). Thus, planetesimals should commonly grow to planetary masses before the disappearance of gas in protoplanetary disks.

The possibilities to overcome the barrier are in principle as follows (their likelihood is commented on below):

1. *Large M*.—Large planetesimals with sizes of 100–1000 km are formed directly in turbulent environments by a mechanism other than collisional coagulation, jumping over the erosive regime for physical radii.

2. *Small* Σ_g.—Planetesimals start their accretion to planet size only after the disk surface density of gas has declined to sufficiently small values.

3. *Small* γ.—Planetesimals form in MRI-inactive regions ("dead zones") of protoplanetary disks.

Concerning point 1, the firstborn planetesimals with sizes larger than R_{acc} may be formed rapidly by an efficient capture of ~meter-sized boulders in vortexes (Johansen et al. 2007; Cuzzi et al. 2008). Such large planetesimals may be consistent with the size distribution of asteroids (Morbidelli et al. 2008). Even if the firstborn planetesimals are not as large, a small fraction of them could continue to grow larger than R_{acc} by accreting smaller bodies, because accretion is not completely cut off as soon as $v_{disp} \gtrsim v_{esc}$ (there is always a small possibility for accretion) and the large planetesimals would not be disrupted by smaller ones. This possibility, however, must be examined by a more detailed growth model taking into account the effect of fragmentation and the size distribution of planetesimals, which we neglected in this paper.

Concerning point 2, we have shown that planetesimals are most fragile at early times, in massive disks, and at large orbital distances. We therefore suggest that the growth toward planet sizes may be delayed due to MRI turbulence and then proceed from inside out; planetesimals should start accretion first close to the star, then progressively at larger orbital distances, as the gas surface density declines. The possibility to delay planet formation while keeping nonmigrating km-sized planetesimals is noteworthy because it would help planetary systems resist type I migration; they would grow in a gas disk that is less dense and for which migration timescales may be considerably increased. Ida & Lin (2008a), Alibert et al. (2005), and Daisaka et al. (2006) showed that type I migration must be lowered by 1–2 orders of magnitude

from the linear calculation (Tanaka et al. 2002) to provide an explanation for the existence of a population of giant planets in agreement with observations. This "late formation" scenario is consistent with the noble gas enrichment in Jupiter (Guillot & Hueso 2006). However, in order to form gas giants, core accretion and gas accretion onto the cores must proceed fast enough to capture a Jupiter-mass amount of gas from the decaying gas disk. Once the size of the largest planetesimals exceeds ~1000 km, their eccentricities are damped by tidal drag and dynamical friction from small bodies. Most of the other small bodies may be ground into sizes smaller than 1 km, and their eccentricities could be kept very small by gas drag and collision damping. This could facilitate the runaway accretion of cores to become large enough ($\gtrsim 10\ M_\oplus$) for the onset of runaway gas accretion. This issue also has to be addressed by a detailed planetesimal growth model taking into account a size distribution. The likelihood of relatively rapid gas accretion without a long "phase 2" is discussed by Shiraishi & Ida (2008). If planetesimal sizes are relatively small, gas drag damping opens up a gap in the planetesimal disk around the orbit of a core and truncates planetesimal accretion onto the core. The truncation of heating due to planetesimal bombardment enables the core to efficiently accrete disk gas.

Concerning point 3, the MRI inactive region ("dead zones") may exist in inner disk regions in which the surface density is large enough to prevent cosmic and X-rays from penetrating the disk (Gammie 1996; Sano et al. 2000). The preservation of a dead zone can also contribute to stall type I migration by converting it to type II migration (Matsumura et al. 2007) or by creating a local region with a positive radial gradient of disk pressure near the ice line (Ida & Lin 2008b). However, dead zones can be eliminated by turbulent mixing/overshoot (Varnière & Tagger 2006; Turner et al. 2007; Ilgner & Nelson 2008), a self-sustaining mechanism (Inutsuka & Sano 2005), and dust growth (Sano et al. 2000). The last effect comes form the fact that small dust grains are the most efficient agents for charge recombination. According to grain growth, the ionization of the disk and its coupling with the magnetic field become stronger to activate MRI turbulence. We remark that if MRI turbulence is activated, collisions are disruptive and they reproduce small grains to decrease the ionization degree. This self-regulation process might maintain a marginally dead state and keep producing small dust grains. This might be related with relative chronological age difference (~2 Myr) between chondrules and calcium-aluminum–rich inclusions (e.g., Kita et al. 2005). Whether dead zones exist or not is one of the biggest issues in the evolution of protoplanetary disks and planet formation. A more detailed analysis of planetesimal accretion in turbulent disks could impose a constraint on this issue.

At large orbital distances (tens of AU), the existence of a highly erosive regime that lasts until late in the evolution of the protoplanetary disk is an important feature of this scenario. It shows that the entire mass of solids is highly reprocessed by collisions, in qualitative agreement with the paucity of presolar grains (intact remnants from the molecular cloud core) found in meteorites. It also prevents the growth of large planetesimals and helps to maintain a large population of small grains in the disks. This is in qualitative agreement with observations that do not indicate a significant depletion of micron-sized grains with time, contrary to what would be predicted in the absence of turbulence (Dullemond & Dominik 2005; Tanaka et al. 2005).

In conclusion, the existence of MRI turbulence may be a threat to planetesimal accretion. Given the uncertainties related to these explanations, we cannot provide a definitive scenario for the formation of protoplanetary cores. However, it offers several promising hints to explain important features of planet formation as constrained by today's observations of protoplanetary disks, exoplanets, and meteoritic samples in the solar system.

This research was supported by the Sakura program between Japan and France and by the CNRS interdisciplinary program "Origine des planètes et de la Vie" through a grant to T. G. and A. M.

APPENDIX

Here we derive the r-dependence in equation (13). If the equation of motion is scaled by a reference radius r_1 and $T_{\rm K,1}$, where $T_{\rm K,1}$ is a Keplerian period at r_1, the only remaining nondimensional parameter in the equations is (see eqs. [4], [5], and [6] in Ogihara et al. 2007)

$$\gamma\Gamma(r_1) = \gamma \frac{64\Sigma_g r^2}{\pi M_\odot}\bigg|_{r_1}. \tag{A1}$$

Consider the equation of motion scaled by r_1 and $T_{\rm K,1}$ and that scaled by r_2 and $T_{\rm K,2}$. If γ is the same and $\Gamma(r_1) = \Gamma(r_2)$, these two scaled equations of motion are identical and the evolution of eccentricity, which is a nondimensional quantity, must be identical in terms of the scaled time. Note that the magnitude of excited e should be proportional to $\gamma\Gamma$. Since

$$\Gamma(r) = \frac{\Sigma_g(r)}{\Sigma_g(r_1)}\left(\frac{r}{r_1}\right)^2 \Gamma(r_1) \tag{A2}$$

and equation (34) of Ogihara et al. (2007) derived for $r = 1$ AU is proportional to $\gamma\Gamma(1\ \mathrm{AU})$, the formula for arbitrary r is given by replacing a year by $T_{\rm K}(r)$ and γ by $\gamma[\Gamma(r)/\Gamma(1\ \mathrm{AU})]$ in their equation. As a result,

$$e \sim 0.1\gamma\left(\frac{\Sigma_g}{\Sigma_{g,1}}\right)\left(\frac{r}{1\ \mathrm{AU}}\right)^2\left(\frac{t}{T_{\rm K}}\right)^{1/2}, \tag{A3}$$

where $\Sigma_{g,1}$ is Σ_g at 1 AU with $f_g = 1$ (eq. [8]) and the numerical factor was corrected as explained in the footnote in § 3.1. Assuming the simple power-law model defined by equation (7),

$$e \sim 0.1 f_g \gamma\left(\frac{r}{1\ \mathrm{AU}}\right)^{-1/4}\left(\frac{t}{1\ \mathrm{yr}}\right)^{1/2}. \tag{A4}$$

REFERENCES

Adachi, I., Nakazawa, K., & Hayashi, C. 1976, PASJ, 29, 163
Alibert, Y., Mousis, O., Mordasini, C., & Benz, W. 2005, ApJ, 626, L57
Balbus, S. A., & Hawley, J. F. 1991, ApJ, 376, 214
Barge, P., & Someria, J. 1995, A&A, 295, L1
Benz, W., & Asphaug, E. 1999, Icarus, 142, 5
Britsch, M., Clarke, C. J., & Lodato, G. 2008, MNRAS, 385, 1067
Cumming, A., Butler, R. P., Marcy, G. W., Vogt, S. S., Wright, J. T., & Fischer, D. A. 2008, PASP, 120, 531
Cuzzi, J., Hogan, R. C., & Shariff, K. 2008, ApJ, in press
Daisaka, K. J., Tanaka, H., & Ida, S. 2006, Icarus, 185, 492
Dullemond, C. P., & Dominik, C. 2005, A&A, 434, 971
Fischer, D. A., & Valenti, J. A. 2005, ApJ, 622, 1102
Gammie, C. F. 1996, ApJ, 457, 355
Goldreich, P., & Ward, W. 1973, ApJ, 183, 1051
Guillot, T., & Hueso, R. 2006, MNRAS, 367, L47
Hayashi, C. 1981, Prog. Theor. Phys. Suppl., 70, 35
Hueso, R., & Guillot, T. 2005, A&A, 442, 703
Ida, S. 1990, Icarus, 88, 129
Ida, S., & Lin, D. N. C. 2005, ApJ, 626, 1045
———. 2008a, ApJ, 673, 487
———. 2008b, ApJ, 658, 584
Ida, S., & Nakazawa, K. 1989, A&A, 224, 303
Ilgner, M., & Nelson, R. P. 2008, A&A, 483, 815
Inutsuka, S., & Sano, T. 2005, ApJ, 628, L155
Johansen, A., Oishi, J. S., Low, M. M., Klahr, H., Thomas, H., & Youdin, A. 2007, Nature, 448, 1022
Johnson, E. T., Goodman, J., & Menou, K. 2006, ApJ, 647, 1413
Kita, N. T., et al. 2005, in ASP Conf. Ser. 341, Chondrites and the Protoplanetary Disk, ed. A. N. Krot, E. R. D. Scott, & B. Reipurth (San Francisco: ASP), 558
Laughlin, G., Steinacker, A., & Adams, F. C. 2004, ApJ, 608, 489
Matsumura, S., Pudritz, R. E., & Thommes, E. W. 2007, ApJ, 660, 1609
Morbidelli, A., Nesvorny, D., Bottke, W. F., & Levison, H. F. 2008, ACM Abstr., submitted
Nelson, R. P. 2005, A&A, 443, 1067
Nelson, R. P., & Papaloizou, J. C. B. 2004, MNRAS, 350, 849
Ogihara, M., Ida, S., & Morbidelli, A. 2007, Icarus, 188, 522
Ohtsuki, K. 1993, Icarus, 106, 228
Rice, W. K. M., & Armitage, P. J. 2003, ApJ, 598, L55
Safronov, V. 1969, Evolution of the Protoplanetary Cloud and Formation of the Earth and Planets (Moscow: Nauka)
Sano, T., Miyama, S. M., Umebayashi, T., & Nakano, T. 2000, ApJ, 543, 486
Santos, N., Israelian, G., & Mayor, M. 2004, A&A, 415, 1153
Shakura, N. I., & Sunyaev, R. A. 1973, A&A, 24, 337
Shiraishi, M., & Ida, S. 2008, ApJ, 684, 1416
Tanaka, H., Himeno, Y., & Ida, S. 2005, ApJ, 625, 414
Tanaka, H., Takeuchi, T., & Ward, W. R. 2002, ApJ, 565, 1257
Tanaka, H., & Ward, W. R. 2004, ApJ, 602, 388
Turner, N. J., Sano, T., & Dziourkevitch, N. 2007, ApJ, 659, 729
Varnière, P., & Tagger, M. 2006, A&A, 446, L13